# A 4H-SiC trench IGBT with controllable hole-extracting path for low loss

Lijuan Wu(吴丽娟)[†], Heng Liu(刘恒), Xuanting Song(宋宣廷), Xing Chen(陈星), Jinsheng Zeng(曾金胜), Tao Qiu(邱滔), and Banghui Zhang(张帮会)

*Hunan Provincial Key Laboratory of Flexible Electronic Materials Genome Engineering, Changsha University of Science & Technology, Changsha* 410114, *China*

(Received 15 April 2022; revised manuscript received 4 July 2022; accepted manuscript online 5 August 2022)

A novel 4H-SiC trench insulated gate bipolar transistor (IGBT) with a controllable hole-extracting (CHE) path is proposed and investigated in this paper. The CHE path is controlled by metal semiconductor gate (MES gate) and metal oxide semiconductor gate (MOS gate) in the p-shield region. The grounded p-shield region can significantly suppress the high electric field around gate oxide in SiC devices, but it weakens the conductivity modulation in the SiC trench IGBT by rapidly sweeping out holes. This effect can be eliminated by introducing the CHE path. The CHE path is pinched off by the high gate bias voltage at on-state to maintain high conductivity modulation and obtain a comparatively low on-state voltage ($V_{ON}$). During the turn-off transient, the CHE path is formed, which contributes to a decreased turn-off loss ($E_{OFF}$). Based on numerical simulation, the $E_{OFF}$ of the proposed IGBT is reduced by 89% compared with the conventional IGBT at the same $V_{ON}$ and the $V_{ON}$ of the proposed IGBT is reduced by 50% compared to the grounded p-shield IGBT at the same $E_{OFF}$. In addition, the average power reduction for the proposed device can be 51.0% to 81.7% and 58.2% to 72.1% with its counterparts at a wide frequency range of 500 Hz to 10 kHz, revealing a great improvement of frequency characteristics.

**Keywords:** controllable hole-extracting path, energy loss, frequency characteristics, SiC insulated gate bipolar transistor (IGBT)

**PACS:** 85.30.De, 85.30.Tv, 85.30.Pq **DOI:** 10.1088/1674-1056/ac8722

## 1. Introduction

SiC materials have excellent characteristics, including wide band gap, high critical electric field, and high electron drift velocity, while insulated gate bipolar transistor (IGBT) combines the characteristic of high current density, making SiC IGBT have immense potential in the field of high voltage and power applications.[1–6] Conventional SiC trench devices are confronted with grim problems of oxide protect. The grounded p-shield region is widely employed in SiC MOSFET. However, in SiC IGBT, this structure will extract holes and weaken conductivity modulation when the device is turned on. Wei *et al*. proposed the diode-clamped p-shield structure and floating p-shield structure for solving this problem.[7,8] Another focused issue is improving the switching characteristic of SiC IGBT, and most approaches are devoted to extracting carriers. A common method is designing extractor in collector region to sweep out electrons,[9–12] but it also leads to low injection efficiency. In addition, the hole extractor is also feasible and it is more compatible with the top process. Sawada *et al*. firstly proposed the hole path concept and designed the hole path controlled by emitter shorted trench gate in floating p-region.[13] Peng *et al.* proposed an adjustable hole path which is controlled by JFET gate.[14] Wei *et al.* proposed a self-adaptive hole-extracting path which controlled by two MOS gates. These above structures can concurrently achieve strong conductivity modulation effect and rapid switching.[15] Therefore, design of hole extraction structures in advanced SiC IGBTs is better.

In this paper, a novel 4H-SiC trench IGBT with CHE path is proposed. The operating mechanism and key parameters of the proposed IGBT is investigated. Considered with its counterparts, the simulated results demonstrate that the studied device presents superior static and dynamic characteristics.

## 2. Device mechanism and description

The SiC conventional IGBT (C-IGBT), the SiC grounded p-shield IGBT (GS-IGBT), and the proposed SiC controllable hole-extracting IGBT (CHE-IGBT) are shown in Fig. 1. These three structures are only changed at the top side region. The grounded p-shield is designed to counteract the electric field peak in trench gate of CHE-IGBT and GS-IGBT. Compared with GS-IGBT, the CHE path is formed in p-shield, which is between the MES gate and MOS gate. The MES gate is formed by Schottky contact. Considering the influence of different Schottky barriers on leakage current, it will be discussed later. In addition, the bottom of MES gate is also packed by thick oxide to decrease leakage currents. The doping concentration in the CHE path is lower than p-shield, and it is connected with the emitter.

The operating mechanism of CHE-IGBT in on-state is plotted in Fig. 1(d). The CHE path is mainly depleted by the MES gate and partially depleted by the MOS gate in on-state.

[†]Corresponding author. E-mail: 413675452@qq.com

© 2023 Chinese Physical Society and IOP Publishing Ltd 

When the CHE path is completely depleted by high gate bias voltages, it can prevent the emitter from extracting holes in drift through p-shield, so as to maintain strong conductivity modulation and low $V_{ON}$ in drift region. With the gate bias voltage switches to negative, the CHE path is reopened in Fig. 1(e). Stored holes will be swept out to the emitter immediately through p-shield at this moment. Furthermore, only a small amount holes will be extracted by the left emitter due to the hole potential barrier between the p-body and carrier storage layer (CSL). With the existence of two hole-extracting paths, the proposed device can turn off swiftly and achieve minimal $E_{OFF}$.

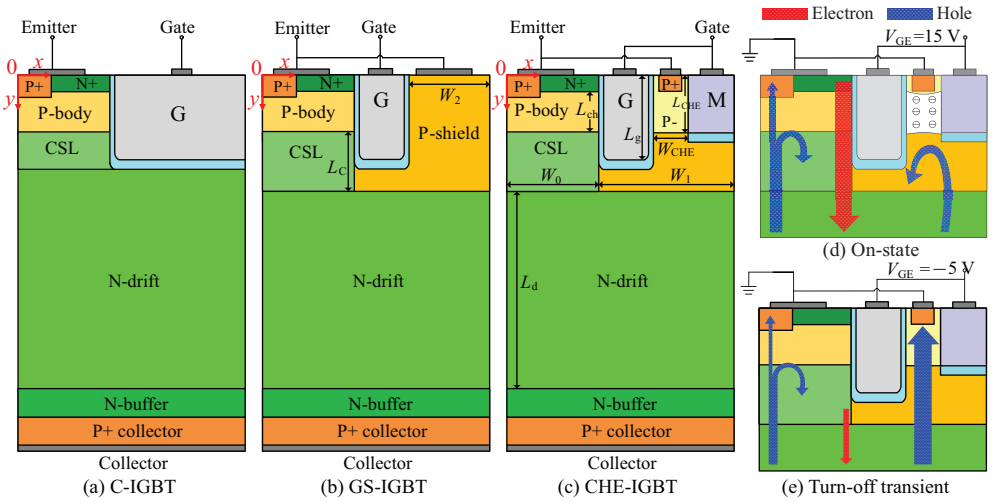



**Fig. 1.** Schematic cross-section of (a) C-IGBT, (b) GS-IGBT, and (c) the proposed CHE-IGBT; operating mechanism of CHE-IGBT in (d) on-state and (e) turn-off transient. When a positive gate bias is applied, the MOS channel turns on and the CHE path turns off. When a negative bias is applied, the opposite is true.

**Table 1.** Key device parameters.

| Parameters | Definitions | Value |
|---|---|---|
| $W$ (μm) | width of CSL layer | 1 |
| $W_1$ (μm) | width of bottom p-shield | 1.6 |
| $W_2$ (μm) | width of top p-shield | 1 |
| $W_{CHE}$ (μm) | width of CHE path | optimized |
| $\gamma$ | ratio of $W_{CHE}$ and $W_2$ | optimized |
| $L_{CHE}$ (μm) | length of CHE path | optimized |
| $L_{ch}$ (μm) | length of channel | 0.5 |
| $L_g$ (μm) | length of gate | 2.1 |
| $L_C$ (μm) | length of CSL | 2 |
| $L_d$ (μm) | length of N-drift | 150 |
| $N_{CHE}$ (μm) | doping of CHE path | optimized |
| $N_{drift}$ (μm) | doping of N-drift | $4.5\times10^{14}$ |
| $N_{CSL}$ ($cm^{-3}$) | doping of CSL | $2\times10^{16}$ |
| $N_{buffer}$ ($cm^{-3}$) | doping of N-buffer | $5\times10^{16}$ |
| $N_{collector}$ ($cm^{-3}$) | doping of P+ collector | $1\times10^{19}$ |
| $N_{shield}$ ($cm^{-3}$) | doping of p-shield | $5\times10^{18}$ |

The key device parameters of the following investigations are shown in Table 1, and these devices' drift parameters are designed for 15-kV voltage level according to Sung *et al.*[16] The thickness of sidewall and bottom of gate oxide is 50 nm and 100 nm, respectively. The mobility of MOS-channel is set to be 30 $cm^2/V{\cdot}s$. And the lifetime of electron and hole is set as 2 μs in simulation. It must be noted that the common physical models of SiC IGBT are employed, including bandgap narrowing model, incomplete ionization model, mobility model (doping and high field dependence); recombination models (Shockley–Read–Hall recombination, Auger recombination, and concentration-dependent lifetime). The above models have been early and continuously applied to 4H-SiC devices.[17–20]

## 3. Electrical characteristics

The p-shield can relieve the reliability of gate oxide in C-IGBT. However, the emitter will extract holes through grounded p-shield in on-state, which causes a large conductive loss. Figure 2(a) shows that a terrible $V_{ON}$ (8.23 V) is obtained in GS-IGBT at $V_{GE} = 15$ V and $I_C = 100$ A/cm$^2$. But C-IGBT gets a low $V_{ON}$ of 3.99 V. For the proposed CHE-IGBT, the CHE path is pinched off, maintaining strong conductivity modulation, which is similar to C-IGBT. Hence, the $V_{ON}$ of the CHE-IGBT is 4.09 V. The hole density of these devices in on-state is plotted in Fig. 2(b), and the proposed CHE-IGBT have the same hole concentration distribution in drift. Due to the existence of grounded p-shield, the lower hole density distribution is shown in GS-IGBT.

During turn-off transients, enhanced conductivity modulation will seriously deteriorate the turn-off time of general SiC IGBTs, since a large number of stored carriers must be removed. The switching test circuit shown in the insert of Fig. 3(a) is utilized to study and discuss turn-off characteristics. The bus voltage is set as 9 kV (60% of 15 kV), and a 2.6 A constant current source is employed to imitate the inductive load circuit. The diode is an ideal component. The gate bias switches from −5 V to 15 V at 10 kHz, and the gate resistor is 10 Ω. These device's areas are set as 0.026 cm$^2$, guaranteeing the operating current density are 100 A/cm$^2$.

Figure 3(a) shows the turn-off waveforms of all the SiC

IGBTs. Compared with C-IGBT, CHE-IGBT and GS-IGBT have similarly excellent switching characteristics. According to the integral of the turn-off curves, the $E_{OFF}$ of the proposed CHE-IGBT, GS-IGBT, and C-IGBT are 2.46 mJ, 2.21 mJ, and 23.02 mJ, respectively. The $E_{OFF}$ of CHE-IGBT is decreased by about 89% compared with C-IGBT.

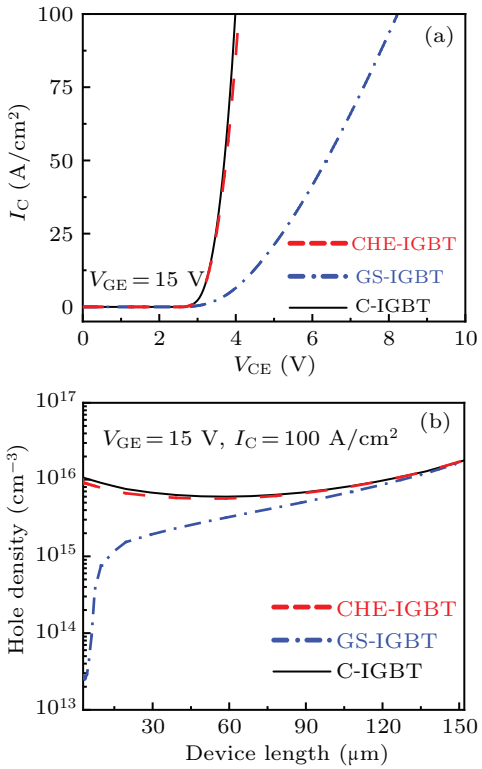



**Fig. 2.** C-IGBT, GS-IGBT and CHE-IGBT's (a) froward *I–V* characteristics and (b) hole density distribution at $I_C$ = 100 A/cm$^2$ and $V_{GE}$ = 15 V. CHE-IGBT has similar $V_{ON}$ and hole density with C-IGBT, but GS-IGBT shows a large $V_{ON}$ and a low hole density.

When all the SiC IGBTs begin to turn off, the space charge region in drift gradually expands to withstand high voltage, and the excessive holes must be extracted in this process. For the C-IGBT, stored holes slowly drawn out by emitter through hole barrier (formed between P-body and CSL layer). Consequently, it takes a long time for the collector to rise from 0 V to the bus voltage $V_{bus}$, resulting in a great $E_{OFF}$. An additional hole extraction path is formed by grounded p-shield, and the hole density in drift is fairly low, so the collector voltage rises very rapidly during turn-off transients in GS-IGBT. In the CHE-IGBT, the CHE path transforms from off to on as the gate bias changes from 15 V to −5 V. Then, excess holes are primarily extracted by emitter through grounded p-shield, and fraction holes are crossing the hole barrier to emitter. Hence, the $E_{OFF}$ is sharply reduced compared with C-IGBT since the existence of controllable hole path.

The tradeoff curve between $V_{ON}$ and $E_{OFF}$ is plotted in Fig. 3(b). At $V_{ON}$ = 4.09 V, the $E_{OFF}$ of CHE-IGBT is decreased by 89% compared with C-IGBT. At the same time, a 50% reduction of $V_{ON}$ is achieved in CHE-IGBT by comparing to GS-IGBT at $E_{OFF}$ = 2.46 mJ. Conclusively, the proposed device can achieve lower total energy loss in practical circuit application.

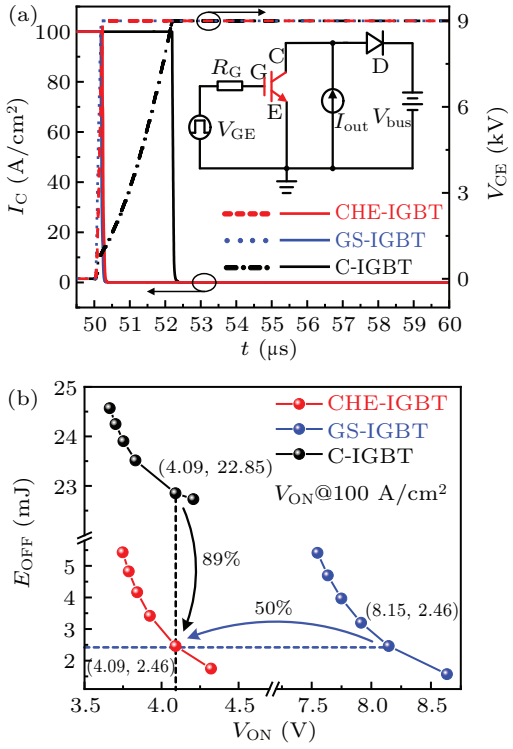



**Fig. 3.** (a) Turn-off waveforms of C-IGBT, GS-IGBT, and CHE-IGBT and (b) tradeoff waveforms between $V_{ON}$ and $E_{OFF}$.

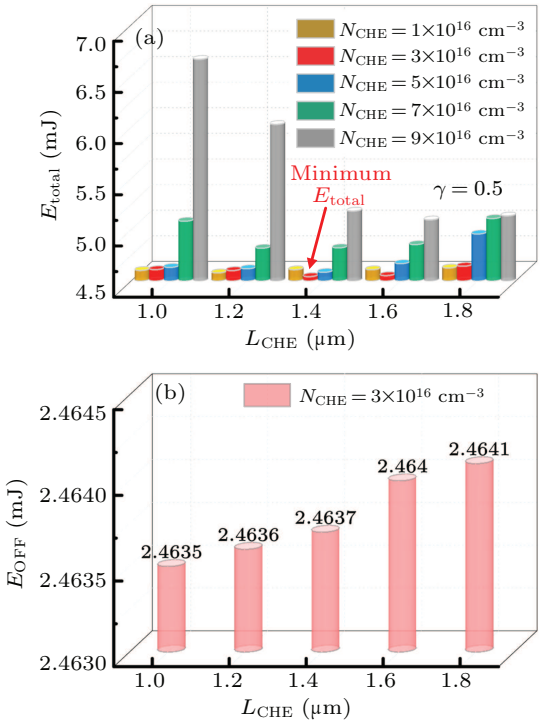



**Fig. 4.** (a) Total energy loss and (b) turn-off loss of CHE-IGBT @10 kHz versus $N_{CHE}$ and $L_{CHE}$ when $\gamma$ = 0.5.

In this paper, the influence of the CHE path parameters (including $L_{CHE}$, $N_{CHE}$, and $\gamma$) on the total energy loss ($E_{total}$) for CHE-IGBT in a cycle is also investigated and simulated.

Assuming $\gamma$ as a scaling factor of the current, the effect of $N_{CHE}$ and $L_{CHE}$ on the $E_{total}$ of the CHE-IGBT can be easily and quickly investigated, and larger $N_{CHE}$ and smaller $L_{CHE}$ will cause the CHE path cannot be completely depleted in on-state, resulting in more conductive loss. The optimization of $E_{total}$ on $N_{CHE}$ and $L_{CHE}$ for the CHE-IGBT with $\gamma = 0.5$ at 10 kHz is shown in Fig. 4(a). The $E_{total}$ decreases with lower $N_{CHE}$ when $L_{CHE} = 1$ μm and 1.2 μm, showing that the proposed device has a good conductive characteristics with small $N_{CHE}$. However, for small $N_{CHE} = 1 \times 10^{16}$ cm$^{-3}$, the CHE path is practically pinched off and leads to slightly increased leakage current with a large $L_{CHE}$, indicating a corresponding rise in conductive loss. Figure 4(b) illustrates that both $N_{CHE}$ and $L_{CHE}$ have little effect on the $E_{OFF}$, indicating conductive loss dominates the optimization in $E_{total}$. The lowest $E_{total}$ of the CHE-IGBT is obtained at the optimized value of $N_{CHE} = 3 \times 10^{16}$ cm$^{-3}$ and $L_{CHE} = 1.4$ μm, which is also selected for a superior performance at operating frequency of 10 kHz.

Figure 5(a) shows the effect of the $E_{total}$ on $\gamma$ with the given $N_{CHE} = 3 \times 10^{16}$ cm$^{-3}$ and $L_{CHE} = 1.4$ μm. Obviously, larger $\gamma$ causes weakened conductivity modulation effect and smaller $\gamma$ leads to leakage currents. Thus, it is explained that the $E_{total}$ will increase with $\gamma$ moving away from the value of 0.5. As shown in Fig. 5(b), the speed of extracting stored holes in turn-off transient is enhanced following the broadened CHE path, resulting in a slightly decreased $E_{OFF}$.

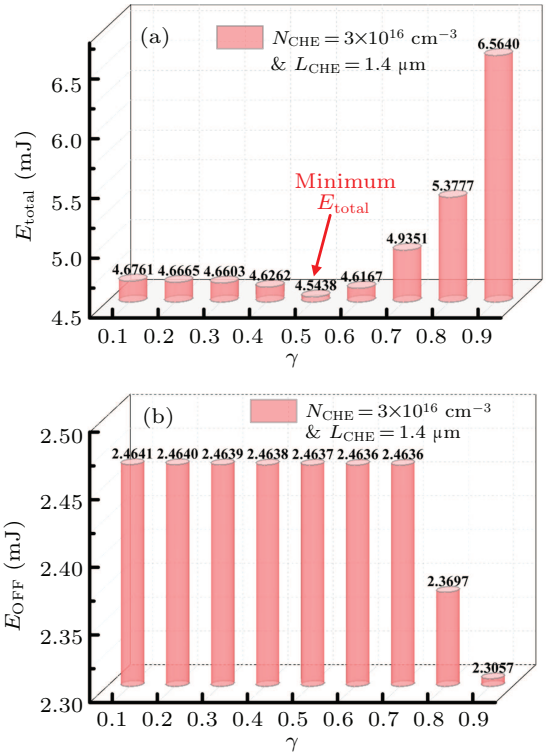



**Fig. 5.** (a) Total energy loss (b) turn-off loss of CHE-IGBT @10 kHz versus $\gamma$, when $N_{CHE} = 3 \times 10^{16}$ cm$^{-3}$ and $L_{CHE} = 1.4$ μm.

The dependence of p-Schottky contact metal on the $E_{total}$ is further investigated by considering the depletion region of the Schottky barrier junction. In the following simulation, the electrode metal of the MES gate is chosen by magnesium, titanium, nickel, and platinum, and their work functions are set as 3.7, 4.2, 5.2, and 5.8, respectively. The effect on $E_{total}$ and $E_{OFF}$ within the chosen material are shown in Fig. 6. It is observed that both $E_{total}$ and $E_{OFF}$ slightly decrease with the increased work functions. The possible reason is that a relatively low p-Schottky barrier is gained when use platinum, which can easily extract a small amount of hole in the turn-off transient. However, the above effect on device is negligible, so the Schottky electrode metal can preferred elect by simplify the manufacturing process.

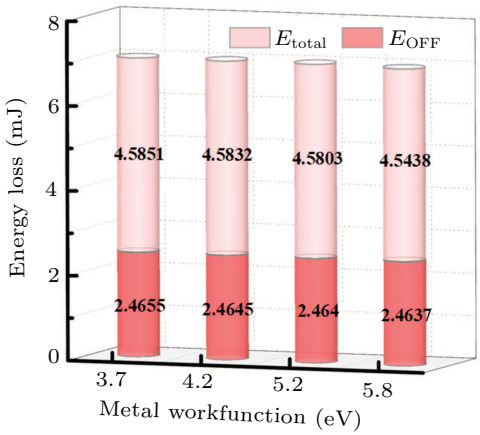



**Fig. 6.** The $E_{total}$ and $E_{OFF}$ of CHE-IGBT @10 kHz at different metal work functions.

Figure 7 shows the effect of different duty ratios (from 10% to 90%) on the average power of all the SiC IGBTs at the operating frequency of 10 kHz. Compared with GS-IGBT and C-IGBT, the average power of the proposed device reduces by 70.5% to 74.0% and 79.7% to 83.8% with the decreased duty ratio, demonstrating the CHE-IGBT is preferred in lower duty ratio signal circuits.

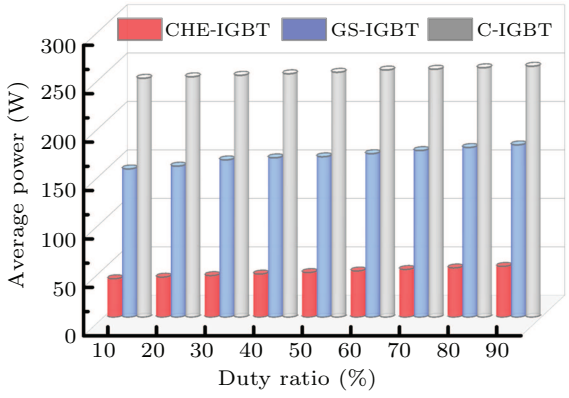



**Fig. 7.** Average power of C-IGBT, GS-IGBT, and CHE-IGBT @10 kHz at different duty ratios.

The wide range operating frequency of 500 Hz to 10 kHz at duty ratio of 50% is selected to investigate the advantage of the proposed device in different circuit applications. In

this comparison, the CHE-IGBTs is optimized at different frequencies by using the previously mentioned method. As discussed above, the CHE-IGBTs have similar conductive power compared with C-IGBT in a wide range frequency in Fig. 8. It is worth explaining that the turn-on power dominates its switching power in GS-IGBT in this simulation, resulting in increased switching power. Although the average power is significantly increased with higher working frequencies, the reduction of the average power of the CHE-IGBTs achieve 58.2% to 72.1% and 51.0% to 81.7% by comparing with its counterparts, respectively. The corresponding CHE path parameters of the optimized CHE-IGBTs in Fig. 8 is listed in Table 2. It is worth indicating that the optimized $\gamma$ and $N_{\rm CHE}$ maintain constant value of 0.5 and $3\times10^{16}$ cm$^{-3}$ from 500 Hz to 10 kHz. Therefore, CHE-IGBTs can be simply fabricated by using the same mask layout when operating at a wider frequency range.

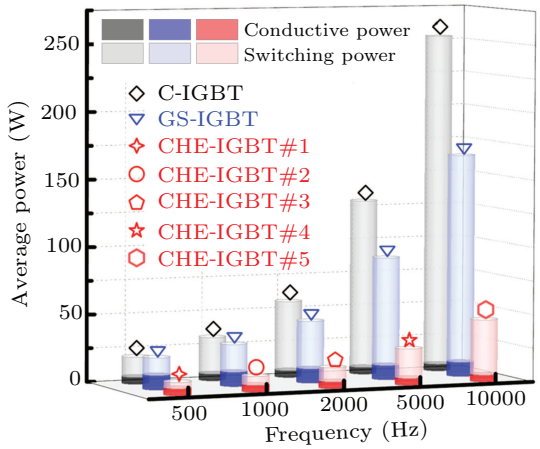



**Fig. 8.** Average power of C-IGBT, GS-IGBT, and the optimized CHE-IGBTs @50% duty ratio at the operating frequency from 500 Hz to 10 kHz.

**Table 2.** Optimized parameters shown in Fig. 8.

| # | $\gamma$ | $N_{\rm CHE}$ (cm$^{-3}$) | $L_{\rm CHE}$ (μm) | Reduced power with GS-IGBT | Reduced power with C-IGBT |
|---|---|---|---|---|---|
| #1 | 0.5 | $3\times10^{16}$ | 1.5 | 58.2% | 51.0% |
| #2 | 0.5 | $3\times10^{16}$ | 1.5 | 62.1% | 63.7% |
| #3 | 0.5 | $3\times10^{16}$ | 1.5 | 66.1% | 72.6% |
| #4 | 0.5 | $3\times10^{16}$ | 1.5 | 70.3% | 79.3% |
| #5 | 0.5 | $3\times10^{16}$ | 1.4 | 72.1% | 81.7% |

## 4. Conclusion

A novel CHE-IGBT featuring a CHE path is proposed and investigated by comparing with C-IGBT and GS-IGBT in this work. The simulation analysis demonstrates that the CHE path can remarkably decrease the $E_{\rm OFF}$ by 89% compared with C-IGBT without sacrificing the $V_{\rm ON,}$ and reduce the $V_{\rm ON}$ by 50% compared to GS-IGBT without sacrificing the $E_{\rm OFF}$, indicating the proposed device can achieve a better $V_{\rm ON}$–$E_{\rm OFF}$ tradeoff. The influence of the CHE path parameters on device performances is also considered. Based on the discussion of the above key parameters, the effect of different duty ratios and operating frequencies on the average power of SiC IGBTs are finally studied. In conclusion, the proposed CHE-IGBT can achieve a less average power in low duty ratio frequency applications by a relatively simple fabrication process.

## Acknowledgements

Project supported by the Hunan Provincial Natural Science Foundation of China (Grant No. 2021JJ30738), Scientific Research Fund of Hunan Provincial Education Department (Grant No. 19K001), and Hunan Provincial Key Laboratory of Flexible Electronic Materials Genome Engineering's Open Fund Project-2020 (Grant No. 202016).

## References

[1] Han L B, Liang L, Kang Y and Qiu Y F 2021 *IEEE Trans. on Power Electron.* **36** 2080
[2] Yonezawa Y 2018 *International Power Electronics Conference*, May 20–24, 2018, Niigata, Japan p. 3603
[3] Chowdhury S and Chow T P 2016 *Proceedings of the 28th International Symposium on Power Semiconductor Devices and ICs*, June 12–16, 2016, Žofín Palace, Prague, p. 75
[4] Fukuda K, Okamoto D, Okamoto M, *et al.* 2015 *IEEE Trans. Electron Dev.* **62** 396
[5] Ryu S, Capell C, Brunt E V, *et al.* 2015 *Semicond. Sci. Technol.* **30** 084001
[6] Östling M, Ghandi R and Zetterling C M 2011 *Proceedings of the 23th International Symposium on Power Semiconductor Devices and ICs*, May 23–26, 2011, San Diego, USA, p. 10
[7] Wei J, Zhang M, Jiang H P, Li B K and Chen K J 2019 *IEEE Trans. on Electron Devices* **66** 3034
[8] Wei J, Zhang M, Jiang H P, To S, Kim S H, Kim J Y and Chen J K 2018 *Proceedings of the 30th International Symposium on Power Semiconductor Devices and ICs*, May 13–17, Chicago, USA, p. 411
[9] Liu Y J, Wang Y, Hao Y, Yu C H and Cao F 2017 *IEEE Trans. Electron Dev.* **64** 488
[10] Liu Y J, Wang Y, Hao Y, Fang J P, Shan C and Cao F 2017 *IEEE Trans. Electron Dev.* **64** 4575
[11] Tang G N, Tang X Y, Song Q W, Yang S, Zhang Y M, Zhang Y M and Zhang Y M 2020 *IEEE Trans. Electron Dev.* **67** 198
[12] Wang Y, Yu C F, Mao H K, Wu X, Su F W, Li X J, Yang J Q 2020 *IEEE Journal of the Electron Devices Society* **8** 1010
[13] Sawada M, Sakurai Y, Ohi K, Ikura Y, Yamazaki T and Nabetani Y 2017 *Proceedings of the 29th International Symposium on Power Semiconductor Devices and IC's (ISPSD)*, May 28–June 1, Sapporo, Japan, p. 65
[14] Peng X, Li Z H, Zhao Y S, *et al.* 2019 *Proceedings of the 31th International Symposium on Power Semiconductor Devices and ICs*, May 19–23, Shanghai, China, p. 51
[15] Wei J, Zhang S, Luo X R, Fan D and Zhang B 2021 *IEEE Trans. Electron Dev.* **68** 2572
[16] Sung W, Wang J, Huang A Q and Baliga B J 2009 *Proceedings of the 21th International Symposium on Power Semiconductor Devices and IC's*, June 14–18, Barcelona, Spain, p. 271
[17] Usman M and Nawaz M 2014 *Solid-State Electron.* **92** 5
[18] Usman M, Buono B and Hallén A 2012 *IEEE Trans. Electron Dev.* **59** 3371
[19] Tamaki T, Walden G G, Sui Y and Cooper J A 2008 *IEEE Trans. Electron Dev.* **55** 1920
[20] Nawaz M and Chimento F 2014 *Mater. Sci. Forum.* **778** 1034